Supporting Information

Ratzke et al. 10.1073/pnas.1000916107

SI Text

Supplemental Methods and Data. *Supplemental methods.*

Experimental setup and data analysis.
All single-molecule fluorescence measurements were performed in a custom-built prism-type total internal reflection fluorescence microscope equipped with two lasers (532 nm Compass 215 M 75 mW, Coherent Inc.; and 635 nm LPM635-25C 25 mW Newport) allowing alternating laser excitation. Fig. S2 shows the setup in more detail. The typical lifetime until photodegradation of the ATTO 647N fluorophore attached to Hsp90 is about 30 s in our system at the intensities of 2–4 mW we used.

To delay photodegradation, we excited the fluorophore only for 100 ms every second, e.g., the minimal time resolution of the presented measurements is 1 s whereas the integration time for every data point (and of several control experiments) is 100 ms. This allowed observation times of several minutes.

In the case of the Coil-NMC construct (where a coiled-coil motif has been added to the N-Terminus to keep the Hsp90 permanently dimerized), the dynamics were so fast that the measurements were done under continuous illumination with an integration time of 100 ms and a time resolution of 110 ms (10-ms readout time of the camera).

The two colors for donor and acceptor fluorescence were separated, filtered, and simultaneously recorded on an Andor DV887 (Andor Technology) camera (Fig. 1*A*). The movies were analyzed with a program from the Hugel Lab based on Igor Pro 6.01 (WaveMetrics): First the time traces of single fluorophores were extracted from Movie S1 with a threshold criterion. Then the two colors were overlaid and the corrected FRET efficiency was calculated (Fig. 1C) according to

$$E_{\mathrm{FRET}} = \frac{I_A}{I_A + \gamma \cdot I_D},$$

where E_{FRET} is the FRET efficiency, I_d and I_a are the donor and acceptor intensities, respectively, and γ is a correction factor that takes the different quantum efficiencies of the dyes and the different detection sensitivity of the setup for the two dyes into account. The γ factor is given as

$$\gamma = \frac{\delta I_A}{\delta I_D},$$

where δI_A and δI_D are changes of acceptor and donor intensities upon acceptor bleaching.

The γ factor was measured for several curves and the average value then has to be taken to correct all FRET curves. The leakage of photons from the donor to the acceptor channel has been estimated to be less than 5%, which would result, for example, in a shift of the low FRET peak from 0.2 to 0.17 after correction or a shift of the high FRET peak from 0.72 to 0.716 after correction. Because of this small effect, the donor leakage has been ignored.

Blinking of the donor is excluded by the stability of the total fluorescence intensity, while the blinking of the acceptor as a source for the observed dynamics is excluded by the fact that the FRET efficiency does not drop to zero as would be the case for blinking, by direct excitation of the acceptor and by alternating excitation experiments.

For the alternating excitation experiments the excitation was 500 ms for every laser, without any dark time between the pulses.

The obtained FRET efficiencies (every single data point) are then cumulated in a histogram as shown in Fig. 1*D*. As fluorescence is a stochastic process, the FRET efficiency of a single state is expected to have a Gaussian distribution. Our efficiencies can very nicely be fit with two Gaussian distributions and can therefore be divided into two states separated at a transfer efficiency of around 0.5. The overlap of the two distributions results in a misassignment of less than 1%. Every crossing by the FRET efficiency curves of this threshold (Fig. 1*E*) corresponds to a transition between the opened and closed states. The dwell times for the open and close events have been plotted in integrated plots that overcome the necessity of data binning (S1). The kinetics were all fitted with the following double exponential:

$$x(t) = 1 + A_1 \cdot e^{-t/\tau_1} + A_2 \cdot e^{-t/\tau_2}.$$

Sample preparation and vesicle encapsulation.
All steps have been carried out in buffer 40 mM Hepes, 150 mM KCl, 10 mM $MgCl_2$, pH 7,5.

The differently labeled Hsp90 dimers have been mixed with a concentration of 200 nm each monomer. After mixing, the heterodimers form in a statistical process, e.g., that 50% of the Hsp90 dimers are heterodimers and 50% acceptor/donor only homodimer, which do not lead to a FRET signal and thus do not disturb the measurement. This solution has been incubated at 37 °C for about 10 min to reach full subunit exchange. To this solution 1,2-Dipentadecanoyl-sn-Glycero-3-Phosphocholine with 1% (n:n) 1,2-Dipalmitoyl-sn-Glycero-3-Phosphoethanolamine-N-(Cap Biotinyl) (Avanti Lipids) to a final concentration of 0.5 μg/μL had been added. This lipid-protein mixture has been pressed at least 30 times through a Mini-Extruders (Avanti Lipids) with a 200-nm pore size polycarbonate-membran (Whatman).

The resulting suspension of unilamellar vesicles with a quite distinct diameter of 200 nM was diluted with measurement buffer to a final mean protein concentration of around 50 pM; the final protein concentration inside the vesicles is around 200 nM per monomer. The nucleotides were added at a concentration of 2 mM to the protein lipid mixture prior to extruding. Thus the nucleotides are also encapsulated by the lipid vesicles. Furthermore, the same nucleotide concentration was added to the surrounding buffer because the melting temperature of the used lipid (33 °C) is quite close to the measurement temperature (30 °C) the vesicles are permeable for the nucleotides and exchange with the surrounding medium can take place (S2).

Exchange experiment.
The subunit exchange experiment was also done in the measurement buffer described above with Hsp90 full-length C560 and Δ8 Hsp90 C560, respectively. All measurements were done at 30 °C —just as the single-molecule measurements. First the Atto550-labeled homodimers were diluted to a concentration of 200 nM and incubated at 30 °C for about 15 min. Then the Atto647N-labeled homodimers were added also at a concentration of 200 nM. The fluorescence has been observed over time in a FP-6500 fluorometer (Jasco) exciting the Atto550 at 530 nm and detecting the Atto550 at 580 nm and the Atto647N at 675 nm. All experiments were done without nucleotides.

Because the concentration of the monomer does not change during the exchange process, the exchange rate should not be concentration dependent. To check this the experiment has been carried out as described at concentrations of 50 nM, 200 nM, 500 nM, and 1000 nM with Δ8Hsp90 C560. The obtained decay

times for a single exponential fit were 509 s for 50 nM, 773 s for 200 nM, 476 s for 500 nM, and 585 s for 1,000 nM. The uncertainties of this bulk experiment are quite large (around 50%), but they are consistent with no pronounced concentration dependence as expected for such a reaction system (depicted in Fig. S6).

Measurement of Förster distance.
The Förster distance in Angström was calculated according to

$$R_0 = \left(9{,}780 \cdot \frac{Q_D \cdot \kappa^2}{n^4} \cdot I\right)^{1/6}$$

with κ as orientation factor set to 2/3 for freely rotating dyes, n the refractive index of water equal to 1.33, Q_D the quantum efficiency of the donor, which is given as $Q_D = \tau_m/\tau_{\mathrm{rad}}$ with τ_m the measured lifetime (see below) in our system, and τ_{rad} the radiative lifetime of the dye. For our system Q was calculated with the assumption of a constant τ_{rad} according to $Q_D = \tau_m/(\tau_{\mathrm{lit}}/Q_{\mathrm{lit}})$ with τ_m the measured fluorescence lifetime and τ_{lit} and Q_{lit} the lifetime and quantum efficiency given by AttoTec for these dyes. The resulting Förster distance for our system is then 5.1 nm. With this the interdye distance is calculated as

$$R = \left(\frac{1 - E_{\mathrm{FRET}}}{E_{\mathrm{FRET}}}\right)^{1/6} \cdot R_0.$$

Lifetime experiments.
Time-correlated single-photon-counting (TCSPC) histograms with 32-ps time bins were measured in a homebuilt microscope similar to other published setups (S3). We use two pulsed diode lasers (532 nm LDH-P-FA-530, PicoQuant, and 640 nm LDH-D-C-640, PicoQuant) as excitation sources, an apochromat 60× water immersion objective (Nikon Instruments) and two single photon avalanched photodiodes (PDM-50 μm, PicoQuant) for green and red fluorescence detection and a commercial data acquisition system (HydraHarp 400, PicoQuant). For the histograms only photon bursts containing more photons than the threshold b are considered. The binning of the photon burst time trace was set to 5 ms in accordance with the diffusion time of HSP90. Black lines show fits to the data using a single exponential function including a background parameter.

1. Gebhardt JC, Clemen AE, Jaud J, Rief M (2006) Myosin-V is a mechanical ratchet. *Proc Natl Acad Sci USA* 103:8680–8685.
2. Cisse I, Okumus B, Joo C, Ha T (2007) Fueling protein DNA interactions inside porous nanocontainers. *Proc Natl Acad Sci USA* 104:12646–12650.
3. Muller BK, Zaychikov E, Brauchle C, Lamb DC (2005) Pulsed interleaved excitation. *Biophys J* 89:3508–3522.

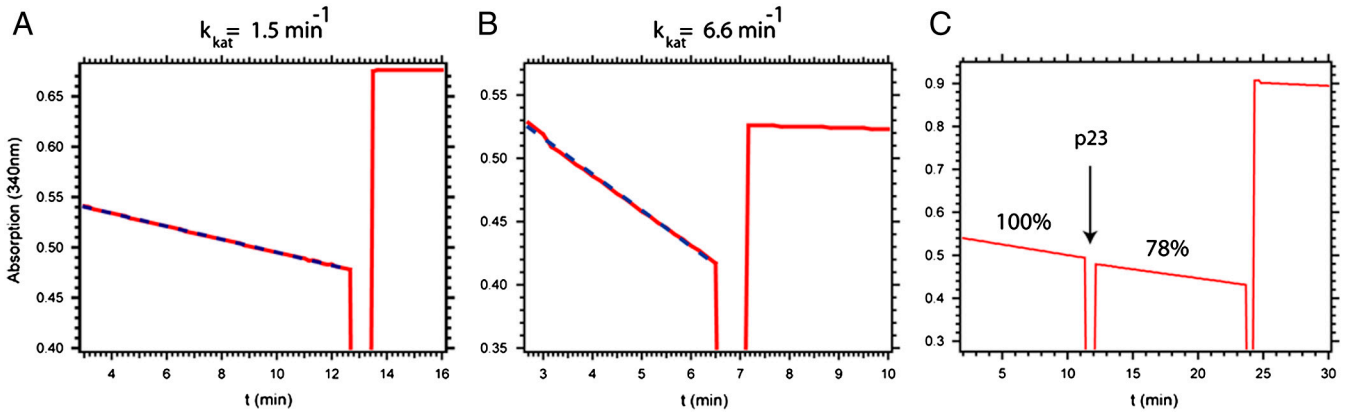

Fig. S1. ATPase Assays. The C560 mutation does not influence the ATPase of any of the constructs within the uncertainty of the measurement. As an example we show in *A* the full-length C560 mutation with normal ATPase activity and inhibition by Radicicol (1) (after around 13 min) and in *B* the Coil-NMC Hsp90 C560 mutant with a higher ATPase activity than the wild-type Hsp90 protein consistent with higher ATPase of Coil-NMC without the C560 mutation. Finally, p23 binding is not inhibited by the C560 mutation, which can be seen in *C*, where the typical ATPase inhibition after p23 addition to Δ8 (C560) can be observed. In the case of Coil-NMC and Δ8 (C560) the labeling process seems to lower the ATPase activity by a factor of 2. This is likely caused by aggregation during the labeling process because the same effect is seen upon the addition of pure DMSO. For the single-molecule experiments, aggregation and inactive protein is irrelevant because we select active single molecules. The ATPase Assay was done with an ATP recovering assay as described in ref. 2. In short the produced ADP is recovered by pyruvate kinase in the presence of posphonenolpyruvate. The produced pyruvate is reduced to lactate by lactate dehydrogenase whereas NADH is oxidizied to NAD^+. The oxidation of NADH leads to a spectral shift and therefore to a change in the absorption at 340 nm with time. This can be observed in the photometer (DU 730, Beckman Coulter). The assay was done at 37 °C. The literature values for the ATPase activity of Hsp90 lie in the range of 0.5–1.5 min^{-1} (3–5). p23 is known to bind to Hsp90 and inhibit the ATPase activity (6). Radicicol is an ATP-mimicking inhibitor that specifically inhibits Hsp90 and thus can be used to estimate the background ATPase activity.

1. Schulte TW, et al. (1998) Antibiotic radicicol binds to the N-terminal domain of Hsp90 and shares important biologic activities with geldanamycin. *Cell Stress Chaperon* 3:100–108.
2. Ali JA, Jackson AP, Howells AJ, Maxwell A (1993) The 43-kilodalton N-terminal fragment of the DNA gyrase B protein hydrolyzes ATP and binds coumarin drugs. *Biochemistry* 32:2717–224.
3. Richter K, Muschler P, Hainzl O, Buchner J (2001) Coordinated ATP hydrolysis by the Hsp90 dimer. *J Biol Chem* 276:33689–33696.
4. Panaretou B, et al. (1998) ATP binding and hydrolysis are essential to the function of the Hsp90 molecular chaperone in vivo. *EMBO J* 17:4829–4836.
5. Wayne N, Bolon DN (2007) Dimerization of Hsp90 is required for in vivo function. Design and analysis of monomers and dimers. *J Biol Chem* 282:35386–35395.
6. Felts SJ, Toft DO (2003) p23, a simple protein with complex activities. *Cell Stress Chaperon* 8:108–113.

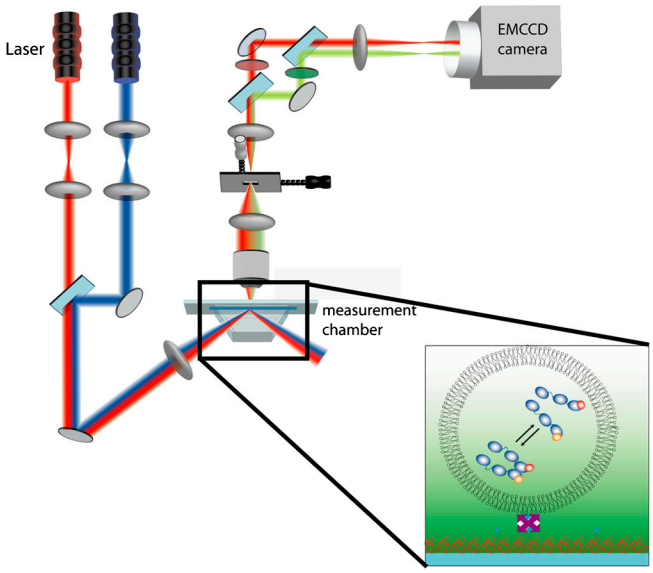

Fig. S2. Single-molecule TIRF setup. The two lasers (532 nm Compass 215 M, 75 mW, Coherent Inc., and 635 nm, LPM635-25C 25 mW, Newport, shown in false color) were collimated by a telescope, then overlaid and directed onto the surface of the measurement chamber via a prisma. The fluorescence light was collected by an objective (Nikon, WI, 1.2 NA). The two colors of the two different dyes were separated by a dichroic mirror and passed through optical band pass filters. After overlaying the two different colors with a slight offset, the beams were directed onto the two halfs of the EMCCD camera. This allows the simultaneous observation of many FRET dyes.

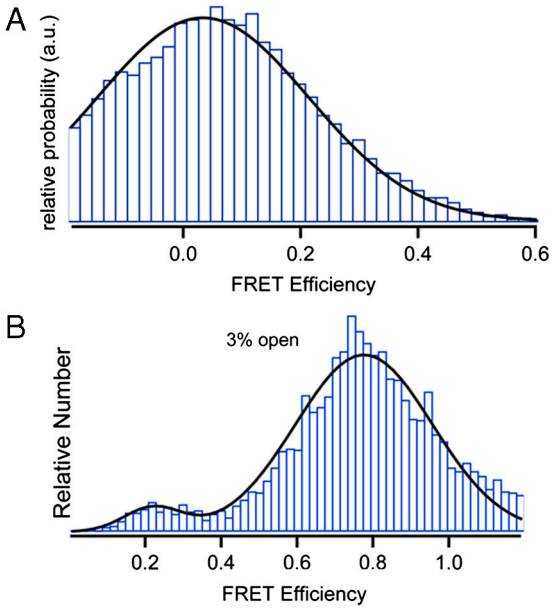

Fig. S3. FRET efficiency histogram of noninteracting dyes and in the presence of Sti1. (*A*) Using heterodimers with one monomer labeled with ATTO 550 at position 61 (in the N terminus) and one monomer labeled with ATTO 647N at position 560 (in the C terminus) an average FRET efficiency of 0.03 was obtained. This shows that the FRET efficiency of 0.2 measured in our C-terminal dynamics experiments does not result from photon leakage of donor photons into the acceptor channel or from unspecific interaction between the proteins. (*B*) The described single-molecule FRET measurements of the C-terminal dimerization have been repeated for the full length Hsp90 in the presence of 1 μM Sti1 (in absence of nucleotide). In this case Hsp90 can be found mainly in the C-terminal closed state. This is consistent with the proposed function of Sti1, which likely binds to the C-terminal domains and opens the N-terminal domains.

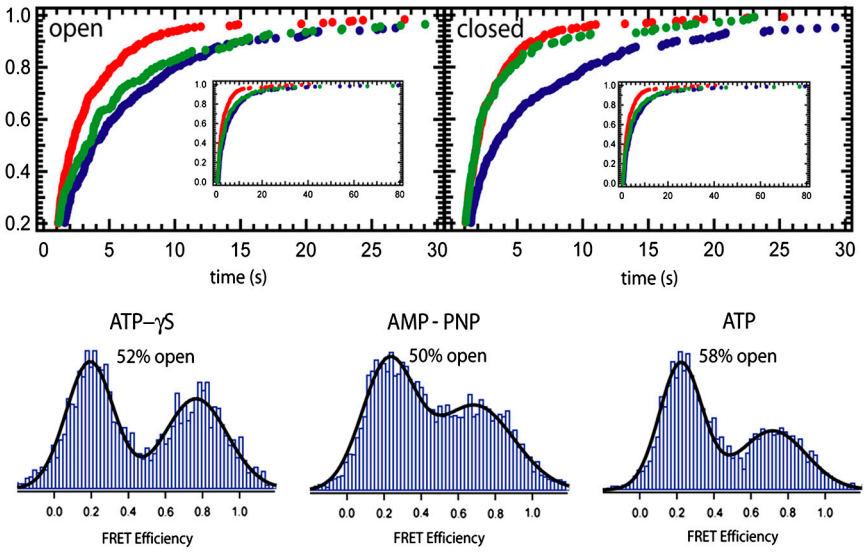

	A_1	τ_1	A_2	τ_{12}	Chi^2
Open					
No	-0,59±0,01	1,45±0,04	-0,43±0,01	10,40±0,61	0,06
ATP	-0,25±0,01	0,79±0,05	-0,72±0,01	5,46±0,15	0,05
ADP	-0,49±0,02	2,96±0,1	-0,48±0,02	12,78±0,6	0,02
γSATP	-0,47±0,03	1,23±0,05	-0,56±0,03	4,03±0,17	0,03
AMP-PNP	-0,23±0,00	0,67±0,03	-0,75±0,00	6,14±0,07	0,03
Closed					
	A_1	τ_1	A_2	τ_2	Chi^2
No	-0,40±0,01	0,85±0,03	-0,60±0,01	8,16±0,2	0,06
ATP	-0,91±0,02	1,54±0,04	-0,20±0,04	20,64±10,5	0,12
ADP	-0,92±0,01	1,01±0,02	-0,16±0,01	10,60±2,62	0,09
γSATP	-0,91±0,15	1,72±0,04	-0,13±0,23	8,04±0,00	0,08
AMP-PNP	-0,37±0,00	0,75±0,01	-0,62±0,00	7,37±0,09	0,02

Fig. S4. Effect of hydrolysis on C-terminal dimerization. FRET efficiency histograms (*Lower*) and integrated dwell-time distributions (*Upper*) in the open and closed states are shown for ATP (green), ATP-γS (red), and adenosine 5′-[β,γ-imido]triphosphate (AMP-PNP) (blue). As the overlap between the two peaks for AMP-PNP is large, the separation of the open and closed states is not always unambiguous, and the open and close times for AMP-PNP should be seen only as rough estimates. The relation between the dissociation constant k_d and the relative amount of closed state α is given in the following: $k_d = [o]/[c]$, $\alpha = [o]/([o] + [c])$ with [o] being the number of open molecules and [c] the number of closed molecules in equilibrium. Together these two equations give $\alpha = k_d/(k_d + 1)$. Changing k_{off} and therefore k_d by a factor of 2 results in a population change from 43% to 59%. This is very close to the values we determined experimentally. The table shows amplitudes (A_i), decay times (τ_i in s), and chi-square values (Chi^2) for all measured nucleotide conditions (No is no nucleotide) of wild-type yeast Hsp90. The decay times for the open states correspond to the on-rate constants and the decay times for the closed states to the off-rate constants.

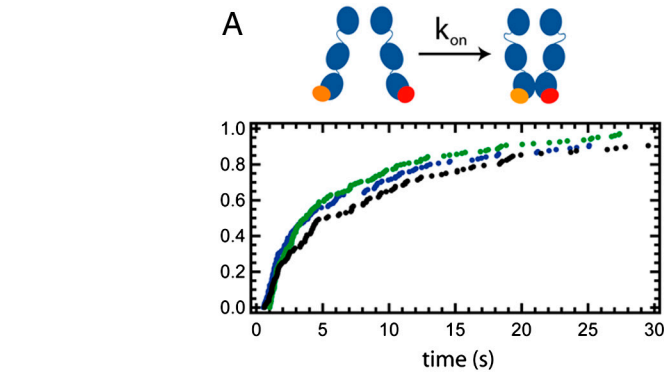

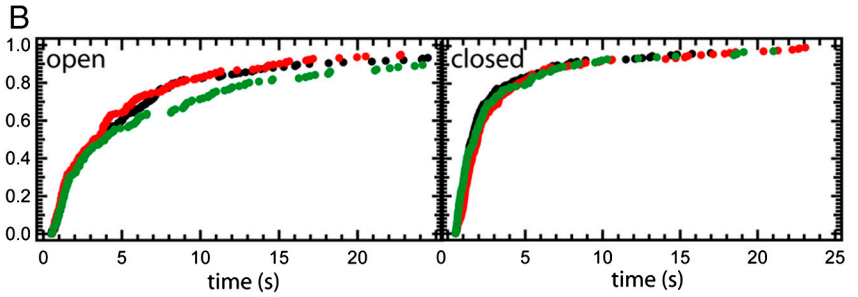

	Open				
	A_1	τ_1	A_2	τ_2	Chi^2
Δ8	-0,26±0,01	0,81±0,07	-0,75±0,01	5,77±0,16	0,07
Δ24	-0,41±0,01	1,21±0,05	-0,59±0,01	11,18±0,35	0,03
Δ8ATP	-0,28±0,01	1,31±0,09	-0,72±0,01	11,82±0,34	0,02
Coil-NMC	-0,37±0,02	0,15±0,02	-0,58±0,02	2,07±0,19	0,03
	Closed				
	A_1	τ_1	A_2	τ_2	Chi^2
Δ8	-0,83±0,01	1,01±0,02	-0,22±0,01	8,42±0,8	0,04
Δ24	-0,66±0,02	0,98±0,03	-0,33±0,01	6,03±0,4	0,02
Δ8ATP	-0,61±0,02	0,49±0,02	-0,37±0,02	3,62±0,33	0,05
Coil-NMC	-0,59±0,03	0,20±0,01	-0,33±0,03	2,27±0,42	0,03

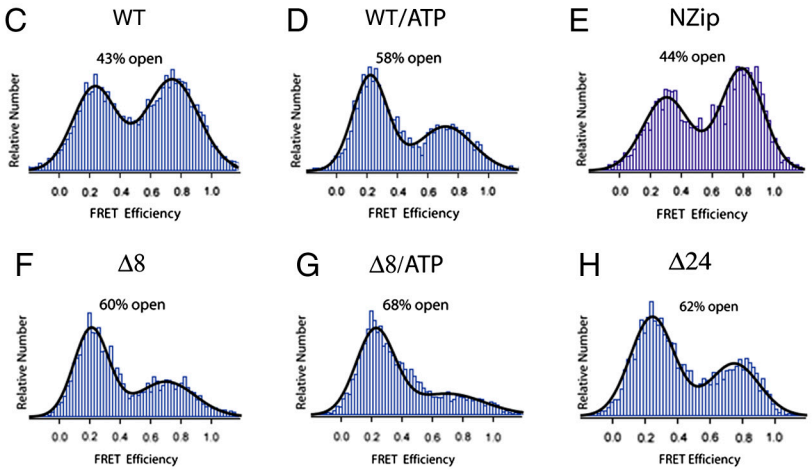

Fig. S5. Effect of N-terminal mutations on C-terminal kinetics. (*A*) Dwell-time distributions for C-terminal open times (k_{on}) are similar for the Δ8 Hsp90 with ATP (N-terminally permanently closed, black), Δ24 Hsp90 (less stable N-terminal dimerization, blue), and wild-type Hsp90 (N-terminal open and closed equilibrium, green). (*B*) Comparison of full-length Hsp90 and the deletion constructs: Dwell-time distributions for Δ8 (black), Δ24 (green) in the absence of nucleotide and the full-length construct in the presence of ATP (red) are very similar. (*Table*) Amplitudes (A_1), decay times (τ in seconds), and chi-square values (Chi^2) for all measured mutants. The τ_1 for the open states correspond to the on-rate constants and the τ_1 for the closed states to the off-rate constants. (*c–f*) C-terminal FRET efficiencies for the different N-terminal mutations. High FRET values correspond to the C-terminal closed state and low FRET values to the C-terminal open state

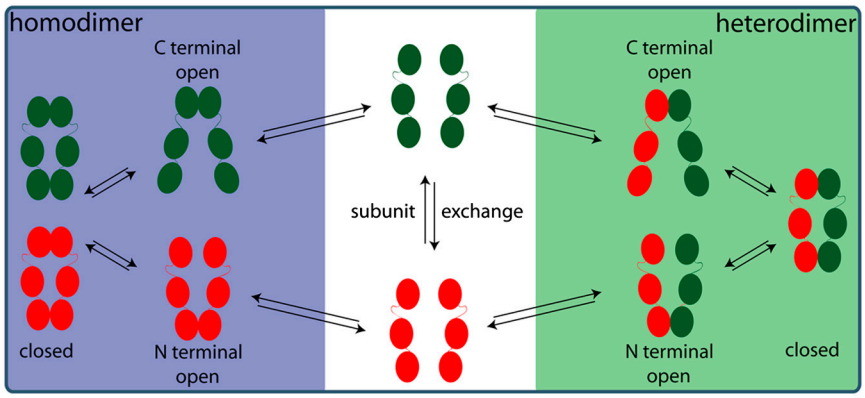

Fig. S6. Reaction pathway scheme for the Hsp90 subunit exchange reaction. The N and C-terminal openings are regarded as independent. The rates are obtained from Fig. S4 and from Mickler et al. (1). In all cases the slowest rates have been chosen.

1. Mickler M, Hessling M, Ratzke C, Buchner J, Hugel T (2009) The large conformational changes of Hsp90 are only weakly coupled to ATP hydrolysis. *Nat Struct Mol Biol* 16:281–286.

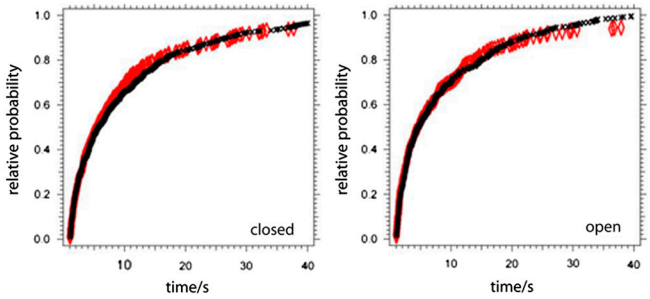

Fig. S7. Comparison of N-N domain vs N-M domain movement. The dynamics of the N-terminal dynamics (red) is the same as can be observed for the N-M domain movement (black), both in the presence of 2 mM ATP. This shows that the N and M domains are quite rigidly linked and move as one unit during the N-terminal opening process. Furthermore, this means that no permanent middle domain interaction takes place and that our results therefore cannot be explained by a holiday junction-like movement.

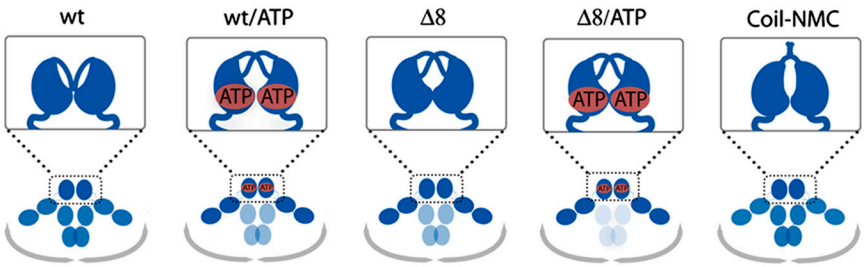

Fig. S8. Scheme of the mechanochemical coupling. Structural model for the position of the N-terminal lid in the various mutants in the presence and absence of ATP. In addition, the occupancy of the C-terminal dimerization equilibrium is given: Dark blue represents high occupancy of the state and light blue represents low occupancy of the state. ATP binding (not hydrolysis) leads to a release of the N-terminal lid, which then can cross-activate the second Hsp90 monomer. In the Δ8 deletion mutant, this process is mimicked (1). So binding of ATP and deletion of the first 8 amino acids lead both to the same effect, namely, the unbinding of the N-terminal lid. This explains why Δ8 mutant and wild type with ATP also show similar C-terminal dynamics.

1. Richter K, et al. (2006) Intrinsic inhibition of the Hsp90 ATPase activity. *J Biol Chem* 281:11301–11311.

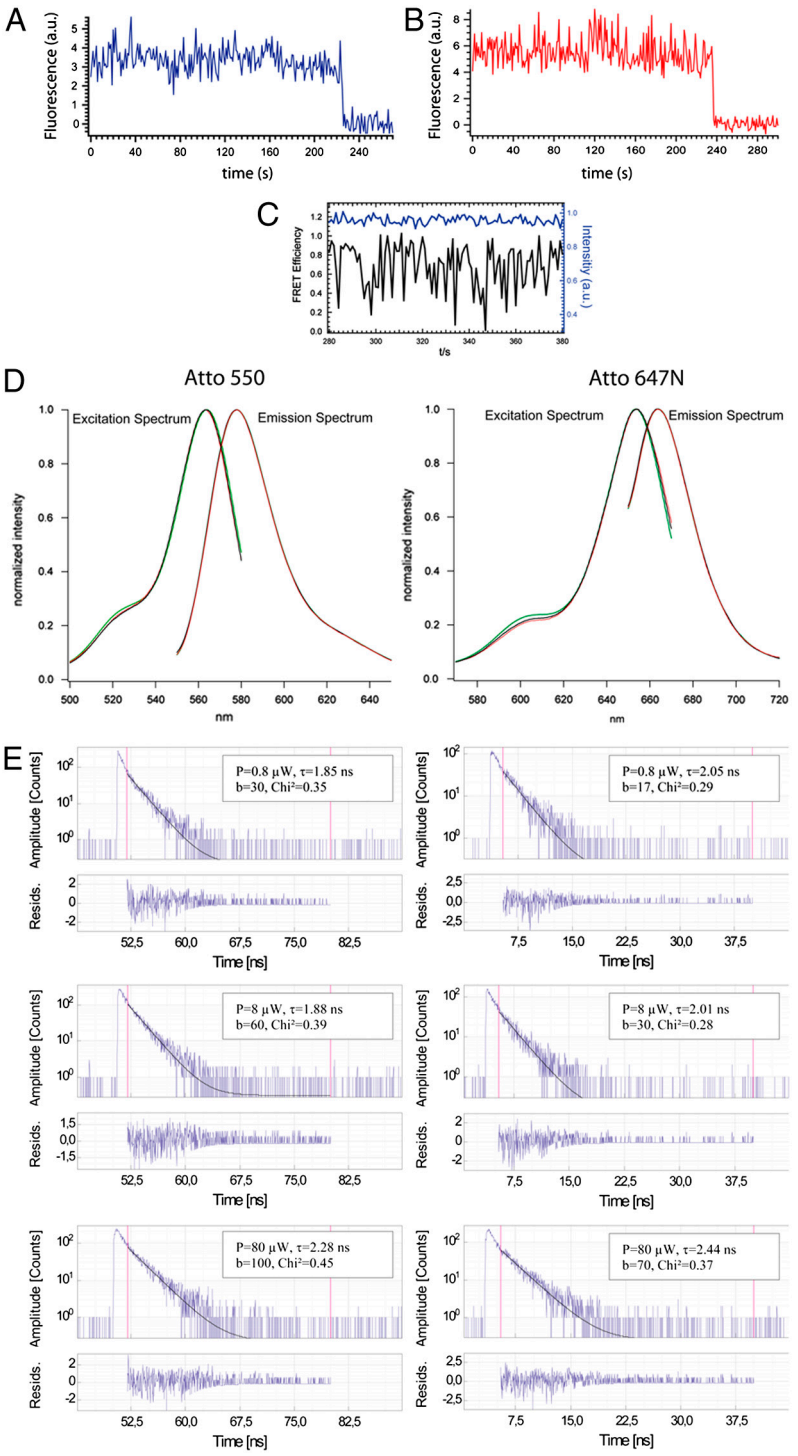

Fig. S9. Test of photostability. (*A*) Total fluorescence intensity of a FRET measurement. Total fluorescence is the corrected sum of donor and acceptor intensity upon donor excitation. The constant signal shows that no donor blinking occurs in the measured time scales. (*B*) Direct excitation of the acceptor dye shows also a stable signal and therefore no blinking of the acceptor. (*C*) Alternating excitation of donor and acceptor dye. Black curve shows the FRET efficiency (at donor excitation); blue curve shows acceptor intensity at direct (acceptor) excitation. As can be seen from this curve, the changes in FRET efficiency are not caused by blinking of the acceptor dye. For detailed description of the experiment, see *Methods*. (*D*) Both dyes were attached to Δ8 Hsp90 C560, spectra were measured at a concentration of 400 nM at 30 °C. The ATTO 550 absorption spectra have been measured at an emission wavelength of 600 nm and the emission spectra with an excitation wavelength of 532 nm, whereas the ATTO 647N absorption spectra have been taken at an emission wavelength of 690 nm and emission spectra with an excitation wavelength of 632 nm. For both dyes the intensities of 2 mW (green), 0.2 mW (black), and 0.1 mW (red) have been used. As can be seen, the emission spectra are the same for all intensities within the uncertainties of this measurement). Therefore this experiment again excludes photophysics as the cause of the observed FRET changes. (*E*) In order to further exclude photophysics as a cause for the observed changes in FRET efficiency, we performed lifetime measurements with our Hsp90 560C constructs at different laser powers P. The lifetime stays constant to at least 8 µw, which is more than 1 order of magnitude higher than the power in our single-molecule FRET experiment. Therefore photophysical effects due to laser power can be excluded in our measurements. The Hsp90 was labeled with ATTO 550 (*Left*) or ATTO 647N (*Right*), respectively. The concentration was about 50 pM for the ATTO 550-labeled HSP90 and about 100 pM for the ATTO 647N-labeled one. τ is the lifetime of the dye obtained from a single exponential fit including background, and b is the burst threshold used for the data. The TCSPC experiments were performed on a homebuilt instrument as detailed in *SI Methods*.

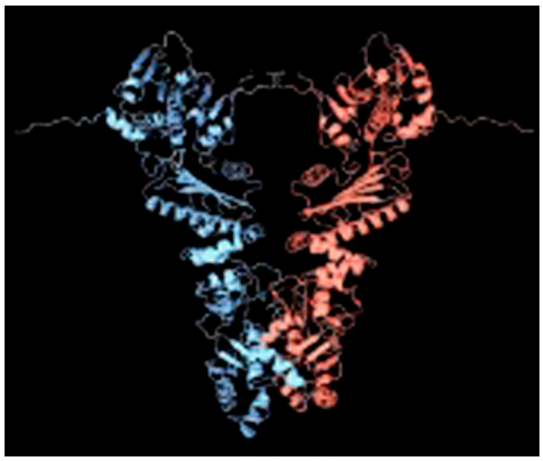

Movie S1. The supplemental movie is a schematic animation of the dynamics of Hsp90. The first part is without nucleotide, then with ATP bound, and finally in the ADP bound state. We determine the rate constants τ_{on} and τ_{off} given in the movie from the integrated dwell-time distributions of this manuscript and our previous work (1). The rate constants are the inverse of the time at which the integrated dwell-time distributions reach half their maximum. Movie made by W. Schürmann, Medienlabor, Technische Universität München.

Movie S1 (MPG)

1. Mickler M, Hessling M, Ratzke C, Buchner J, Hugel T (2009) The large conformational changes of Hsp90 are only weakly coupled to ATP hydrolysis. *Nat Struct Mol Biol* 16:281–286.